PALEOCEANOGRAPHY

Revisiting the mid-Pleistocene transition ocean circulation crisis

Sophia K. V. Hines[1]*, Christopher D. Charles[2], Aidan Starr[3,4], Steven L. Goldstein[5,6], Sidney R. Hemming[5,6], Ian R. Hall[7], Nambiyathodi Lathika[8], Mollie Passacantando[9], Louise Bolge[5]

The mid-Pleistocene transition (MPT) [~1.25 to 0.85 million years ago (Ma)] marks a shift in the character of glacial-interglacial climate (*1*, *2*). One prevailing hypothesis for the origin of the MPT is that glacial deep ocean circulation fundamentally changed, marked by a circulation "crisis" at ~0.90 Ma (marine isotope stages 24 to 22) (*3*). Using high-resolution paired neodymium, carbon, and oxygen isotope data from the South Atlantic Ocean (Cape Basin) across the MPT, we find no evidence of a substantial change in deep ocean circulation. Before and during the early MPT (~1.30 to 1.12 Ma), the glacial deep ocean variability closely resembled that of the most recent glacial cycle. The carbon storage facilitated by developing deep ocean stratification across the MPT required only modest circulation adjustments.

The ice age cycles characteristic of the Pleistocene were the well-known product of changes in Earth's orbit around the Sun, which drives variations in the amount and location of solar radiation reaching Earth's surface (*4*, *5*). Yet, there are several enduring mysteries surrounding the evolution of ice age cycles. In the early Pleistocene, glacial-interglacial cycles occurred at a period of ~41 thousand years (kyr), responding linearly to solar forcing (*5*). Over the mid-Pleistocene transition (MPT), glacial-interglacial cycles lengthened to a period of ~100 kyr. They developed more-intense glacial maxima, reflected by larger ice volumes and sawtooth shapes, thereby responding nonlinearly to solar forcing. This transition in glacial periodicity has been investigated extensively, but a definitive cause remains elusive (*6*).

One leading hypothesis to explain the MPT involves shifts in deep ocean circulation that resulted from changes in the proportion of northern-sourced water (NSW) [the paleo equivalent of modern North Atlantic Deep Water (NADW)] compared with southern-sourced water (SSW) [the paleo equivalent of modern Antarctic Bottom Water (AABW)] in the deep ocean. Initial support for such a shift came from authigenic neodymium (Nd) isotope measurements in a suite of eastern South Atlantic sedimentary sequences: A state change in the amplitude of glacial-interglacial water mass variability was inferred after a missing interglacial Nd isotope shift between marine isotope stage (MIS) 24 and MIS 22 (*3*). This interval also featured a "failed termination" at the MIS 24–MIS 23 transition (TXI), the residual ice from which likely contributed to the marked increase in global ice volume observed over the subsequent MIS 22 glacial [the "0.9 Ma event"; (*7*)]. Subsequent studies have suggested that the characteristic pattern of Nd isotopic variability extended to the North Atlantic (*8*, *9*) and may have been connected with inferences of permanently elevated nutrient and dissolved carbon levels in the deep ocean (*10*).

In this work, we use a new, highly resolved Nd isotope record co-registered with benthic stable carbon and oxygen isotopic time series to demonstrate that the hypothesis of a circulation crisis across this interval must be revised. We present an ~5-kyr-resolution εNd record across the MPT [~1.3 to 0.75 million years ago (Ma)] and ~1-kyr-resolution stable benthic carbon and oxygen isotope records for the past ~1.3 Ma from International Ocean Discovery Program (IODP) site U1479 (2615-m water depth, 35.059°S, 17.401°E) in the South Atlantic, Cape Basin. Site U1479 lies within the main pathway of NADW export from the Atlantic Ocean to the modern Southern Ocean; thus, it is ideally placed to record variability in NSW over the MPT (Fig. 1). We use these three independent proxies of water mass properties to show that, although Northern Hemisphere–driven changes in the production of NSW are often used to explain past water mass variations, the Southern Ocean was likely more important for driving the observed changes in MPT deep ocean water mass structure in the deep Atlantic. The Southern Ocean influence could have occurred directly, through changes that helped set the density of SSW (*11*–*15*), and/or indirectly, through processes that helped to define the density contrasts between NSW and SSW (*16*, *17*). This perspective highlights the importance of cooling on the Antarctic continent and its adjacent ocean (*18*) in preconditioning the late Pleistocene ocean toward longer ice age intervals with increased deep ocean carbon storage; these effects were not previously fully appreciated.

The authigenic Nd isotope composition of marine sediments (reported as εNd, the normalized $^{143}Nd/^{144}Nd$ composition in parts per ten thousand; see materials and methods) is a proxy for deep ocean circulation (*19*). Neodymium enters the ocean primarily by means of rivers, dust deposition, and exchange with continental margin sediments, so the isotopic composition of seawater is set by the isotopic composition of the surrounding continents, which vary as a function of their age and composition. The oldest rocks surrounding the Atlantic basin with the most negative εNd values are found in Canada and Greenland, and they imprint seawater in the North Atlantic Ocean with isotopic values around −13 to −14 (*20*, *21*). Conversely, the youngest rocks with the most positive εNd values are found around the Pacific rim, and they imprint seawater in the Pacific Ocean with isotopic values around −3 to −4 (*22*). Because Nd isotopes are not affected by biology, εNd values of open ocean intermediate and deep waters at least to a first order behave conservatively in many parts of the global oceans, reflecting water mass mixing between these North Atlantic and Pacific Ocean end-members (*20*, *23*–*25*) (Fig. 1A). At a given location, variations in εNd can potentially be complicated by temporal changes in the εNd value of the end-members, but on long timescales (100 kyr to 100 million years), data indicate stable secular North Atlantic and Pacific end-member compositions (*3*). However, this may not be the case over shorter millennial and orbital timescales, particularly for the North Atlantic end-member. Neodymium isotope measurements over the last glacial cycle indicate much more variability in the North Atlantic end-member (*26*, *27*) compared with the Pacific end-member (*28*), possibly driven by Laurentide ice sheet dynamics, which affect the flux of continental material (with very negative εNd compositions) into the North Atlantic Ocean.

Circulation variability across the MPT compared with the last glacial cycle

Our εNd data from site U1479 (Fig. 2) show clear glacial-interglacial cycles that mimic benthic $\delta^{18}O$ and $\delta^{13}C$ variability (fig. S2). Previous studies have suggested substantial shifts in deep ocean circulation across the MPT, recorded at nearby Ocean Drilling Program (ODP) sites 1088, 1090, and 1267 (*3*, *10*), and such shifts should also be reflected in the εNd composition of site U1479. However, comparing our

[1]Department of Marine Chemistry & Geochemistry, Woods Hole Oceanographic Institution, Woods Hole, MA, USA. [2]Scripps Institution of Oceanography, La Jolla, CA, USA. [3]Department of Marine and Coastal Sciences, Rutgers University, New Brunswick, NJ, USA. [4]Department of Geography, University of Cambridge, Cambridge, UK. [5]Lamont-Doherty Earth Observatory, Columbia University, Palisades, NY, USA. [6]Department of Earth and Environmental Sciences, Columbia University, New York, NY, USA. [7]School of Earth and Environmental Sciences, Cardiff University, Cardiff, Wales, UK. [8]National Centre for Polar and Ocean Research, Ministry of Earth Sciences, Goa, India. [9]Graduate School of Oceanography, University of Rhode Island, Narragansett, RI, USA.
*Corresponding author. Email: shines@whoi.edu

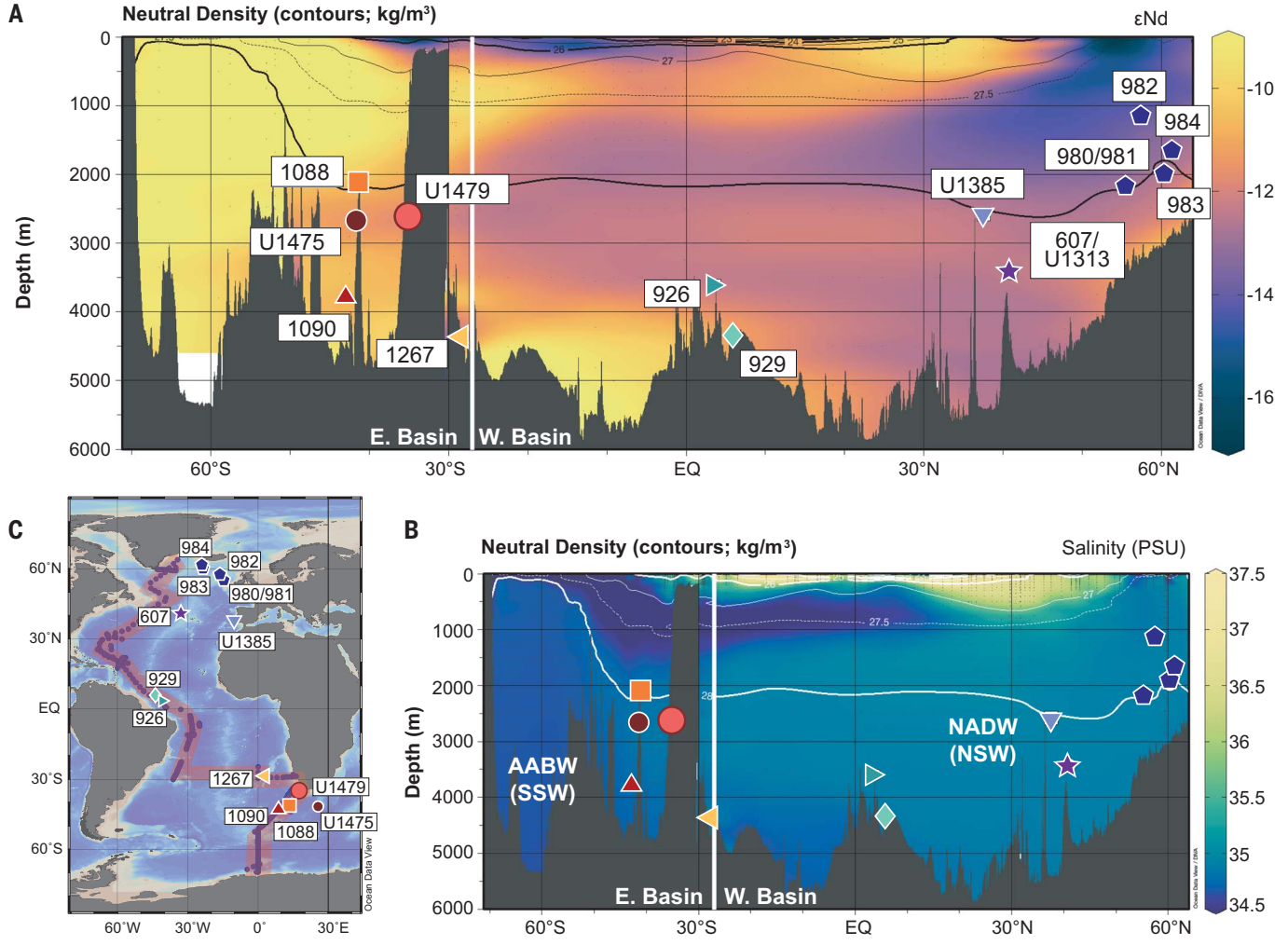

Fig. 1. Atlantic Ocean hydrography with core sites. (**A**) A depth-latitude εNd section through the Atlantic (*20*, *23*–*25*, *52*), with neutral density contours following the red outlined path in (C), crossing from the western to the eastern basin at ~30°S. Site U1479 (this study) is marked with a pink circle. Other sites discussed in the text are also marked. EQ, equator. (**B**) A salinity section with neutral density contours following the same path as in (A). (**C**) Sediment core sites plotted in map view with the transect from (A) and (B) marked. Small blue dots mark seawater Nd isotope stations.

data and a published εNd record over the past 155 kyr from the same site (*29*) reveals a notably similar amplitude of glacial-interglacial εNd variability between the last glacial cycle and the MPT. Glacial εNd values before 1.12 Ma are statistically indistinguishable from glacial values for the past 155 kyr (P = 0.3818 at the 99% significance level). Nd isotope data from the last glacial cycle at site U1479 (*29*) have demonstrated the suitability of this location for deep ocean circulation reconstructions (supplementary text) and provide a valuable framework for comparison because more is known about ocean circulation over the last glacial cycle than during the MPT.

Neodymium isotope values for the Holocene and the last interglacial MIS 5e (median value of −10 with a 25 to 75 percentile range of −9.8 to −10.5) are very similar to interglacial values across the MPT interval (median of −10.6 with a 25 to 75 percentile range of −10.3 to −11; Fig. 2C). εNd values for the Last Glacial Maximum (LGM) and MIS 6 (median of −8.6 with a 25 to 75 percentile range of −8.3 to −8.7) are similar to glacial values between 1.30 and 0.70 Ma (median of −9.1 with a 25 to 75 percentile range of −8.8 to −10.1). During the mid-MPT, between ~1.12 to 0.95 Ma, there is reduced εNd variability and a shift toward more negative εNd values (median of −10.9 with a 25 to 75 percentile range of −10.3 to −11.1) for both glacial and interglacial periods. This interval ends with a notably positive glacial εNd signature of −8.1 during MIS 24 (~0.92 Ma) and an intermediate εNd signature of −9.6 at MIS 23 (~0.90 Ma). To determine whether water mass shifts or end-member changes drive the Nd variability recorded at site U1479, independent information about the εNd value of the North Atlantic end-member is needed. Although a comprehensive deconvolution of end-member changes and water mass mixing is not possible at present because of the resolution of existing data from the North Atlantic (supplementary text and fig. S5), we argue that end-member variability is unlikely to be the primary control of the εNd signal at site U1479 given the strong covariation of εNd with $\delta^{13}C$, another deep ocean circulation proxy (Fig. 3 and fig. S2).

The prevailing MPT circulation hypothesis (*3*) is based on two key interpretations of existing data: (i) an unprecedented weakening in NSW production between MIS 24 and MIS 22 and (ii) an increase in glacial-interglacial water mass variability across the MPT. Our data from site U1479 do not support either of these interpretations. First, given its $\delta^{18}O$ composition and the εNd values that are characteristic of an intermediate climate state (fig. S2), MIS

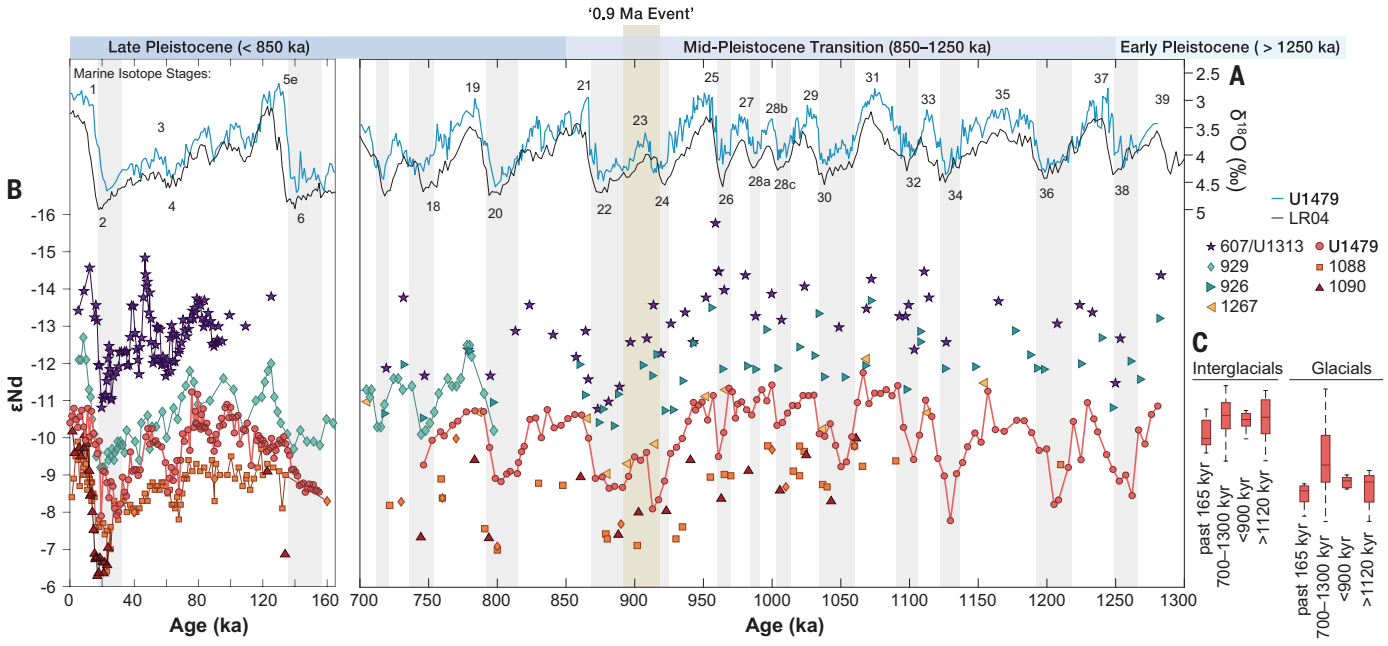

Fig. 2. εNd data for the last glacial cycle and MPT from across the Atlantic Ocean. (**A**) Benthic stable oxygen isotope data from site U1479 (light blue; this study) (*29*) and the LR04 benthic stack (black) (*1*) with marine isotope stages marked. ka, thousand years ago. (**B**) εNd data from across the Atlantic basin for sites 607 and U1313 (purple stars) (*8*, *27*), 929 (light teal diamonds) (*53*), 926 (dark teal right-facing triangles) (*9*), 1267 (yellow left-facing triangles) (*10*), U1479 (pink circles and bold line; this study) (*29*), 1088 (orange squares; orange diamonds mark bulk leach samples) (*3*, *54*, *55*), and 1090 (red triangles) (*3*, *55*). Glacial intervals are marked by gray vertical bars, and the 0.9 Ma event during MIS 23 is marked with a tan vertical bar. (**C**) Glacial and interglacial εNd box plots at site U1479 (pink) for different time intervals.

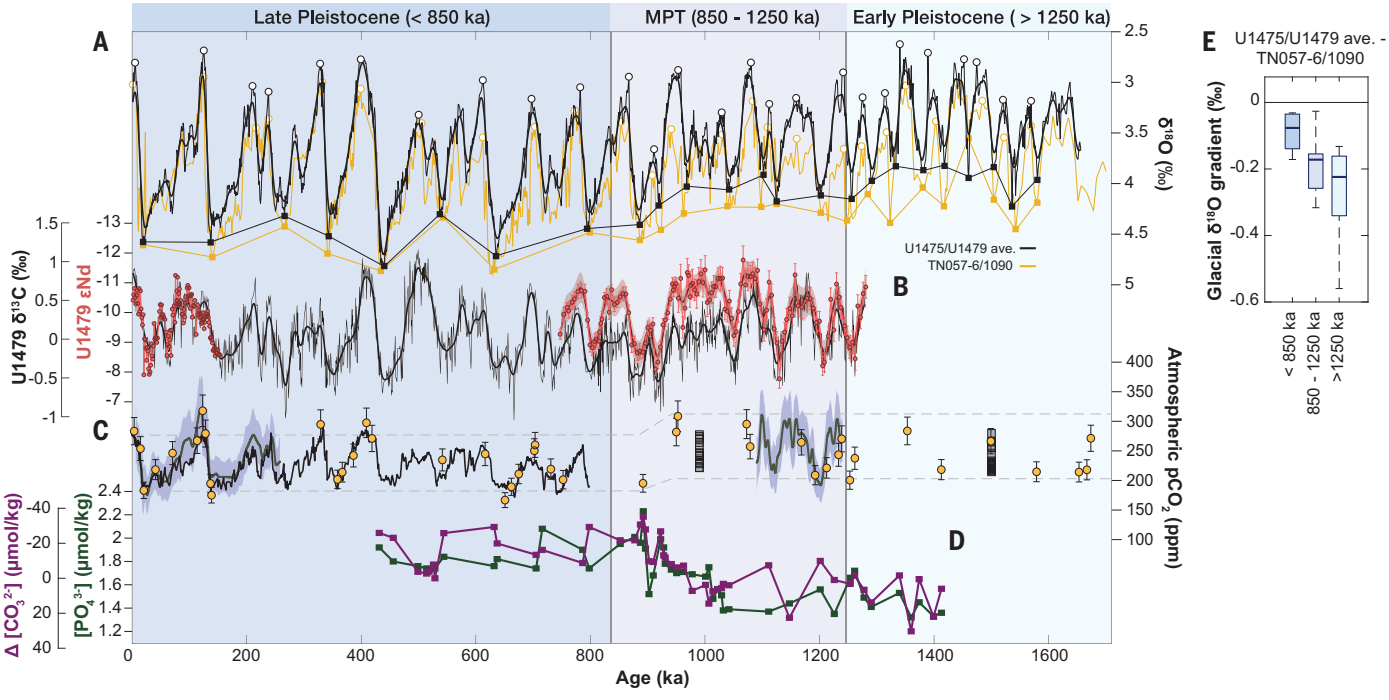

Fig. 3. Ocean circulation and carbon cycle changes over the past 1.5 Ma. (**A**) Benthic stable oxygen isotope data combined from sites U1479 (this study) and U1475 (*16*) (black; see materials and methods) and spliced data from site 1090 and TN057-6 (yellow) (*41*). Filled squares mark glacial maxima and open circles mark interglacial maxima; these points are used to calculate vertical isotope gradients. (**B**) εNd (pink) and benthic $\delta^{13}C$ (black) data from site U1479 over the past ~1.3 Ma. (**C**) Atmospheric pCO_2 records from Epica Dome C in Antarctica (black solid line) (*56*), Allen Hills [gray squares, (*32*, *33*)], and boron isotope measurements [yellow circles, (*30*); gray line and shading, (*31*)]. ppm, parts per million. (**D**) Deep ocean phosphate (green) and carbonate ion (maroon) records from site 1267 (*10*). (**E**) Box plot of vertical oxygen isotope gradient during glacial maxima. Gradients were calculated at glacial maxima (filled squares) between the combined record from sites U1479 and U1475 and the spliced data from site 1090 and TN057-6.

23 should not be regarded as a full interglacial; nevertheless, there is a well-resolved εNd peak at ~0.90 Ma at site U1479 that confirms substantial NSW influence in the South Atlantic during MIS 23 (Fig. 2B). Second, the U1479 record shows no evidence for a state change in the amplitude of deep ocean circulation tracers before and after the MPT: Although it is true that the εNd record is less variable in the ~1.05 to 0.94 Ma interval than over subsequent ice age cycles, the preceding interval (~1.25 to 1.05 Ma) was characterized by cycles in εNd and $\delta^{13}C$ that were equally as strong as post-MPT counterparts.

The importance of high-resolution sampling

The differences between these insights from U1479 and the interpretations from prior records likely stem from sampling resolution and length of record considered. For example, lower sampling resolution of previous reconstructions (*3*, *10*) would have missed the relatively brief interval of low εNd during MIS 23, leading to the inappropriately generalized interpretation of a substantial reduction in NSW production. Furthermore, the interpretation that the amplitude of glacial-interglacial circulation variability changed across the MPT was also based on shorter and/or lower-resolution εNd records (*3*, *8*, *10*). Our reconstruction from site U1479 comprises co-registered stable isotope and εNd data, and therefore, we can observe explicitly that $\delta^{18}O$ maxima and minima did not always correspond with εNd and $\delta^{13}C$ maxima and minima (fig. S4). This inexact correlation precludes an accurate assessment of glacial-interglacial circulation variability if εNd variability is defined strictly on the basis of $\delta^{18}O$ values. A corollary is that data aliasing is a substantial concern when complete glacial-interglacial cycles are not measured at a resolution that captures the full variability. Finally, any pre- and post-MPT comparisons that focus exclusively on the interval immediately surrounding 0.9 Ma will yield a biased perspective. The explanations for reduced variability during the 1.05 to 0.94 Ma interval in U1479 are not yet obvious but could involve localized sampling resolution issues (fig. S5) as well as possible shifts in the Nd isotopic value of the NSW end-member (Fig. 2B and fig. S3) (*8*, *9*).

In any case, the perspective from U1479 bears on a number of aspects of MPT climate variability. Although the range of reconstructed atmospheric pCO_2 before the MPT is large and uncertain, the preponderance of evidence suggests a reduction in glacial pCO_2 across the MPT (*30*–*34*). This evidence is consistent with apparent trends in deep ocean carbon storage (*10*) and deep ocean nutrient and dissolved inorganic carbon concentrations, both of which increased during ice ages through the MPT (Fig. 3, C and D, and fig. S9). Such characteristic trends in carbon cycling have commonly been attributed to a substantial reorganization of deep ocean circulation. However, because the site U1479 record shows that glacial-interglacial circulation variability in the early MPT closely resembled the variability observed during the last glacial cycle, the U1479 results might paradoxically appear to indicate a decoupling of deep circulation and ocean carbon storage: Although changes in biological export can increase carbon removal from the atmosphere and storage in the deep ocean (*35*), efficient carbon storage on long timescales almost certainly requires changes in physical ocean circulation to prevent the return of this respired carbon to the upper ocean and atmosphere (*36*–*40*).

Evolution of deep ocean stratification across the MPT

The clue to resolving this seeming paradox comes from the LGM water mass geometry. High-resolution benthic $\delta^{13}C$ and Nd isotope data from the Cape Basin over the last glacial cycle demonstrate that geochemical gradients, indicative of increased density stratification, can develop between the mid-depth (~2500 m) and abyssal (>4000 m) ocean despite a relatively strong signature of NSW at site U1479 (*29*) (supplementary text). The vertical εNd profile indicates that the depth of the NSW maximum did not shoal substantially (by <500 m) at the LGM. However, there was still a strengthening of the εNd gradient between

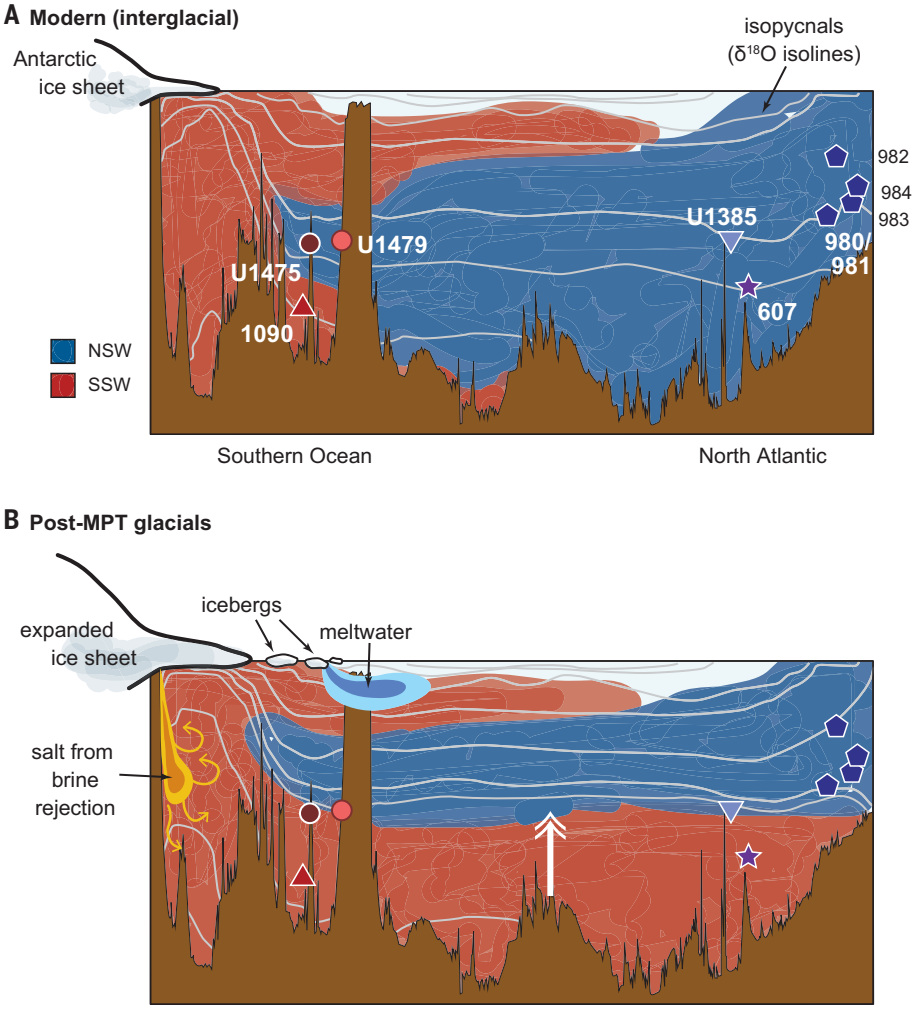

Fig. 4. Ocean circulation changes during the MPT. (**A**) Modern ocean circulation with locations of key sites marked. Light gray lines are isopycnals, which also constitute lines of constant $\delta^{18}O$, and colors mark water masses (NSW, blue; SSW, red). (**B**) Glacial ocean circulation configuration after the MPT, with increased stratification between NSW and SSW (isopycnals lie close together). Site U1479 is near the boundary between NSW and SSW, sharing a water mass with site 1090 such that these sites have similar $\delta^{18}O$ values. Fresh meltwater from Antarctic icebergs may have contributed to enhanced stratification between NSW and SSW by lowering the density of NSW with the addition of fresh meltwater while expanding Antarctic ice sheets and increasing sea ice production, which increased the density of SSW through salt from brine rejection. The overall result is an increase in the NSW-SSW density contrast.

the mid-depth and abyssal ocean driven by the shoaling of the boundary between NSW and SSW, with much less NSW in the deepest part of the Atlantic Ocean. The long-term evolution of deep density stratification over the past ~1.5 Ma can be more directly assessed using benthic oxygen isotope data from the Cape Basin because the $\delta^{18}O$ composition of carbonates is a function of temperature and the $\delta^{18}O$ composition of seawater, which itself is a function of salinity, and seawater density is controlled by temperature and salinity (Fig. 3A). Combining benthic $\delta^{18}O$ data from U1479 with published data from nearby site U1475 (2669-m water depth) (*16*) and comparing this with data from ODP site 1090 (3702-m water depth) (*41*) (Fig. 1) clearly shows that the vertical glacial $\delta^{18}O$ gradients decreased over the MPT, continuing a trend that extends from the early Pleistocene and Pliocene (*42*). The vertical benthic $\delta^{18}O$ difference was ~0.22 per mil (‰) in the early Pleistocene (>1.25 Ma), decreased slightly to ~0.2‰ during the MPT (1.25 to 0.85 Ma), then dropped to >0.1‰ in the Late Pleistocene (<0.85 Ma) (Fig. 3, A and E). The convergence of benthic $\delta^{18}O$ data from the combined U1475 and U1479 record with site 1090 was primarily driven by an increase in the benthic $\delta^{18}O$ recorded at sites U1475 and U1479. This could be explained by a rise in the density of NSW (driven by either a cooling and/or salinity increase) or an expansion of SSW such that this water mass reached the depth of sites U1475 and U1479. Although some reconstructions indicate NSW cooling over this interval (*43*, *44*), an expansion of SSW and shoaling of the boundary between NSW and SSW is the likely explanation because it would provide a more extensive deep ocean reservoir for carbon storage, which increases at this time (Fig. 3D) (*10*). If, instead, the density of NSW increased, the result would be a reduction in the density contrast between NSW and SSW, reducing stratification and inhibiting carbon storage. Therefore, we favor an explanation where the isotopic convergence is driven by SSW expansion and a shoaling of the boundary of NSW and SSW, also characteristic of increased density stratification between NSW and SSW (Fig. 4B).

The evolution of vertical oxygen isotope gradients in the Cape Basin is also consistent with benthic $\delta^{13}C$ gradients from across the Atlantic Ocean (fig. S8). As glacial deep ocean stratification between NSW and SSW develops in the Cape Basin during the MIS 24–MIS 22 interval, ~0.90 Ma, the lateral $\delta^{13}C$ gradient between site U1479 and site U1385 on the Iberian Margin (*45*) in the mid-latitude North Atlantic decreases. At the same time, the $\delta^{13}C$ gradient between site U1385 and the higher-latitude North Atlantic sites 980/1, 982, 983, and 984 (*46*) increases. This observation also favors an expansion of SSW and an increase in mid-depth density stratification rather than an increase in the density of NSW. If the density of NSW increased, this water mass would reach both the high-latitude and mid-latitude North Atlantic sites, potentially placing them all on the same density surface and making it difficult to sustain a $\delta^{13}C$ gradient between these regions because ocean tracers (i.e., benthic $\delta^{13}C$ values) mix easily along density surfaces. Therefore, as density stratification develops in the South Atlantic (characterized by a convergence of benthic $\delta^{18}O$ records at site 1090 and sites U1475 and U1479), it also affects the entire Atlantic basin and increases the volume of deep water available to store carbon during glacials (*47*). Physically, the only way to do this is through changes in the Southern Ocean, which effectively controls the density structure of the deep Atlantic Ocean (*11*, *12*).

The data presented in this work highlight the power of the deep ocean to sequester CO_2 without substantial changes in circulation geometry. This sequestration could be achieved partially through increases in biological productivity, possibly driven by increased iron fertilization in the Southern Ocean (*48*), but changes in ocean stratification apparently played an important role. We suggest that the Southern Ocean was the ultimate driver of deep ocean evolution across the MPT. The Southern Ocean is the central dynamical control of deep ocean stratification, primarily through changes in sea ice production (*11*, *12*, *49*). Deep ocean stratification changes, which occurred at the end of the MPT and are characterized by the expansion of SSW, are best explained as a by-product of cooling (*18*) and the expansion of Antarctic ice sheets (*50*, *51*). Density contrasts between NSW and SSW would also be accentuated by increased iceberg production around Antarctica, through freshwater associated with iceberg melt at the northern edge of the Southern Ocean (*16*) (fig. S9). This perspective on a threshold interval of Pleistocene ice age cycling bears on the evolution of future climate under anthropogenic forcing. Much of the focus when it comes to future climate change is on Atlantic meridional overturning circulation perturbations driven by heat and freshwater fluxes to the North Atlantic. Yet, as the MPT interval suggests, the capacity of the deep ocean to store carbon for long timescales might be much more strongly linked to changes in the Southern Ocean.

REFERENCES AND NOTES

1. L. E. Lisiecki, M. E. Raymo, *Paleoceanography* **20**, PA1003 (2005).
2. P. U. Clark *et al*., *Quat. Sci. Rev.* **25**, 3150–3184 (2006).
3. L. D. Pena, S. L. Goldstein, *Science* **345**, 318–322 (2014).
4. M. Milanković, *Kanon Der Erdbestrahlung Und Seine Anwendung Auf Das Eiszeitenproblem* (Royal Serbian Academy, 1941).
5. J. Imbrie *et al*., *Paleoceanography* **7**, 701–738 (1992).
6. E. Legrain, F. Parrenin, E. Capron, *Commun. Earth Environ.* **4**, 90 (2023).
7. P. C. Tzedakis, M. Crucifix, T. Mitsui, E. W. Wolff, *Nature* **542**, 427–432 (2017).
8. J. Kim *et al*., *Quat. Sci. Rev.* **269**, 107146 (2021).
9. M. Yehudai *et al*., *Proc. Natl. Acad. Sci. U.S.A.* **118**, e2020260118 (2021).
10. J. R. Farmer *et al*., *Nat. Geosci.* **12**, 355–360 (2019).
11. M. Nikurashin, G. Vallis, *J. Phys. Oceanogr.* **41**, 485–502 (2011).
12. C. L. Wolfe, P. Cessi, *J. Phys. Oceanogr.* **40**, 1520–1538 (2010).
13. J. Marshall, K. Speer, *Nat. Geosci.* **5**, 171–180 (2012).
14. R. Ferrari *et al*., *Proc. Natl. Acad. Sci. U.S.A.* **111**, 8753–8758 (2014).
15. A. Marzocchi, M. F. Jansen, *Geophys. Res. Lett.* **44**, 6286–6295 (2017).
16. A. Starr *et al*., *Nature* **589**, 236–241 (2021).
17. F. J. C. Peeters *et al*., *Nature* **430**, 661–665 (2004).
18. P. U. Clark, J. D. Shakun, Y. Rosenthal, P. Köhler, P. J. Bartlein, *Science* **383**, 884–890 (2024).
19. S. L. Goldstein, S. R. Hemming, in *Treatise on Geochemistry*, vol. 6, H. D. Holland, K. K. Turekian, Eds. (Elsevier, 2003), pp. 453–489.
20. M. Lambelet *et al*., *Geochim. Cosmochim. Acta* **177**, 1–29 (2016).
21. S. Robinson *et al*., *Chem. Geol.* **567**, 120119 (2021).
22. Y. Wu, "Investigating the Applications of Neodymium Isotopic Compositions and Rare Earth Elements as Water Mass Tracers in the South Atlantic and North Pacific," thesis, Columbia University (2019).
23. E. Garcia-Solsona *et al*., *Geochim. Cosmochim. Acta* **125**, 351–372 (2014).
24. P. Rahlf *et al*., *Earth Planet. Sci. Lett.* **530**, 115944 (2019).
25. Y. Wu *et al*., *Earth Planet. Sci. Lett.* **599**, 117846 (2022).
26. N. Zhao *et al*., *Nat. Commun.* **10**, 5773 (2019).
27. F. Pöppelmeier *et al*., *Geophys. Res. Lett.* **48**, e2021GL092722 (2021).
28. R. Hu, A. M. Piotrowski, *Nat. Commun.* **9**, 4709 (2018).
29. S. K. V. Hines *et al*., *Paleoceanogr. Paleoclimatol.* **36**, e2021PA004281 (2021).
30. B. Hönisch, N. G. Hemming, D. Archer, M. Siddall, J. F. McManus, *Science* **324**, 1551–1554 (2009).
31. T. B. Chalk *et al*., *Proc. Natl. Acad. Sci. U.S.A.* **114**, 13114–13119 (2017).
32. Y. Yan *et al*., *Nature* **574**, 663–666 (2019).
33. J. A. Higgins *et al*., *Proc. Natl. Acad. Sci. U.S.A.* **112**, 6887–6891 (2015).
34. M. Yamamoto *et al*., *Nat. Geosci.* **15**, 307–313 (2022).
35. D. M. Sigman, M. P. Hain, G. H. Haug, *Nature* **466**, 47–55 (2010).
36. F. Knox, M. B. McElroy, *J. Geophys. Res.* **89**, 4629–4637 (1984).
37. U. Siegenthaler, T. Wenk, *Nature* **308**, 624–626 (1984).
38. J. L. Sarmiento, J. R. Toggweiler, *Nature* **308**, 621–624 (1984).
39. J. R. Toggweiler, J. L. Russell, S. R. Carson, *Paleoceanography* **21**, PA2005 (2006).
40. A. M. De Boer, A. M. C. Hogg, *Geophys. Res. Lett.* **41**, 4277–4284 (2014).
41. D. A. Hodell, K. A. Venz, C. D. Charles, U. S. Ninnemann, *Geochem. Geophys. Geosyst.* **4**, 1–19 (2003).
42. M. O. Patterson *et al*., *Paleoceanogr. Paleoclimatol.* **33**, 825–839 (2018).
43. H. L. Ford, S. M. Sosdian, Y. Rosenthal, M. E. Raymo, *Quat. Sci. Rev.* **148**, 222–233 (2016).
44. S. Sosdian, Y. Rosenthal, *Science* **325**, 306–310 (2009).
45. N. C. Thomas, H. J. Bradbury, D. A. Hodell, *Science* **377**, 654–659 (2022).
46. M. E. Raymo *et al*., *Paleoceanography* **19**, PA2008 (2004).
47. L. C. Skinner, *Clim. Past* **5**, 537–550 (2009).
48. A. Martínez-Garcia *et al*., *Nature* **476**, 312–315 (2011).
49. L.-P. Nadeau, R. Ferrari, M. F. Jansen, *J. Climate* **32**, 2537–2551 (2019).
50. M. E. Raymo, L. E. Lisiecki, K. H. Nisancioglu, *Science* **313**, 492–495 (2006).
51. J. Sutter *et al*., *Cryosphere* **13**, 2023–2041 (2019).
52. R. Schlitzer *et al*., *Chem. Geol.* **493**, 210–223 (2018).
53. J. N. W. Howe, A. M. Piotrowski, *Nat. Commun.* **8**, 2003 (2017).
54. V. Dausmann, M. Frank, M. Gutjahr, J. Rickli, *Paleoceanography* **32**, 265–283 (2017).
55. R. Hu *et al*., *Earth Planet. Sci. Lett.* **455**, 106–114 (2016).
56. D. Lüthi *et al*., *Nature* **453**, 379–382 (2008).
57. S. K. V. Hines, Cape Basin Authigenic Nd and Benthic Stable Isotope Data for the Mid-Pleistocene Transition,

noaa-ocean-39722, NOAA/WDS Paleo Archive (2024); https://www.ncei.noaa.gov/access/paleo-search/study/39722.

ACKNOWLEDGMENTS

This research uses samples provide by the IODP and would not have been possible without the efforts of the Expedition 361 Scientific Party and the JOIDES Resolution technical staff and crew. **Funding:** This study was supported by National Science Foundation grant OCE-1831415 (S.R.H., S.L.G., and S.K.V.H.). **Author contributions:** Conceptualization: S.R.H., S.L.G., C.D.C., and S.K.V.H. Methodology: S.K.V.H., M.P., L.B., and C.D.C. Funding acquisition: S.R.H. and S.L.G. Supervision: S.R.H., S.L.G., and S.K.V.H. Writing – original draft: S.K.V.H. Writing – review & editing: All authors. **Competing interests:** The authors declare that they have no competing interests. **Data and materials availability:** All data are available in the main text, the supplementary materials, or the NOAA/WDS Paleo Archive (*57*).

SUPPLEMENTARY MATERIALS

science.org/doi/10.1126/science.adn4154
Materials and Methods
Supplementary Text
Figs. S1 to S9
References (*58*–*62*)
Data S1 and S2

Submitted 8 December 2023; accepted 4 October 2024
10.1126/science.adn4154